Reducing the effective point spread function in echo planar imaging through the use of partial Fourier asymmetric spin echo pulse sequences

A. S. Nencka[1], D. L. Shefchik[1], E. S. Paulson[2], A. Jesmanowicz[1], and J. S. Hyde[1]
[1]Department of Biophysics, Medical College of Wisconsin, Milwaukee, WI, United States, [2]Department of Radiation Oncology, Medical College of Wisconsin, Milwaukee, WI, United States

Introduction:

A method is presented to improve the point spread function associated with intra-acquisition decay in echo planar imaging (EPI). Although affording increased temporal resolution, acquisition methods that include collecting multiple k-space lines for each excitation suffer from transverse magnetization decay over the course of the readout. In gradient recalled echo (GRE) acquisitions utilizing EPI, T_2* decay effectively limits the duration of acceptable readout echo trains. The decay over the course of the acquisition in k-space leads to an effective convolution in image space with the Fourier transform of the decay function, and thus preferential blurring in the phase encoding direction [1].

Multiple methods have been described to address the blurring issue associated with T_2* decay in EPI, while maintaining the appropriate T_2' contrast corresponding to the selected echo time of the GRE sequence. Partial Fourier and parallel acquisitions can reduce the effective blurring in the phase encoding direction by allowing the intra-acquisition decay to occur over only one half of the traditional readout duration [2,3]. Multi-shot, segmented EPI methods reduce the readout duration by spreading the acquisition over several excitations, thereby reducing the possible temporal resolution [4]. Segmented, multi-echo pulse sequences utilizing a GRE followed by asymmetric spin echoes have also been utilized to reduce the blurring associated with T_2* decay in GRE EPI [5]. In this abstract, we describe a partial Fourier, asymmetric spin echo method to reduce blurring which performs better than standard partial Fourier GRE EPI, and does not suffer from the increased scan time associated with multi-shot GRE EPI.

Theory:

The T_2* decay associated with GRE EPI is comprised of components which can be recovered with a spin echo, T_2', and which cannot be recovered with a spin echo, T_2, such that $1/T_2^* = 1/T_2' + 1/T_2$. When an asymmetric spin echo is acquired, the T_2 and T_2' effects are in competition with each other during the time between the pi pulse and the time at which the spin echo occurs. Thus, the slope of the intra-acquisition decay curve is minimized during this period, yielding a flatter k-space windowing function and, thus, a narrower image-space convolution kernel. Data acquired during this period will yield the minimized reconstructed point spread function in the phase encoding direction. Data acquired immediately following the excitation or the spin echo will experience enhanced blurring associated with T_2* decay.

Methods:

A simulation was run to illustrate the effective decay envelope of an asymmetric spin echo pulse sequence, with 90 ms T_2, 72 ms T_2', 40 ms T_2*, and the π pulse being applied 50 ms after initial excitation.

Dual echo experimental data were acquired on a phantom with partial Fourier asymmetric spin echo readouts on each side of the spin echo, using a General Electric Signa LX 3.0 T imager. The second readout was a temporally reversed copy of the first, allowing each k-space line to have matching T_2' weightings. The parameters for the pulse sequence included: 214.56 ms spin echo time, 20 ms effective GRE echo time, 128x128 acquisition matrix, 16 overscan lines, 240 mm field of view, 7 mm slice thickness, and 2000 ms repetition time. A mean image of 120 repetitions was computed for each asymmetric spin echo, and plots through high contrast regions in the phase and frequency encoding directions were made for each reconstructed image.

Results:

Figure 1 shows the signal intensity envelope that results from the simulation. The slope of the decay envelope during the ascending edge of the spin echo is less than the slopes of the decay envelope before the pi pulse and after the spin echo. It can be shown that if T_2 is equal to T_2', then the slope of the decay envelope on the ascending edge of the spin echo is zero.

Figures 2 and 3 illustrate the time series mean image for data acquired on the ascending side of the spin echo and the descending side of the spin echo, respectively in the phantom. Through the experimental design, T_2' weighting should be matched in these images because of the matched effective GRE echo times. It is apparent that the point spread function in the phase encoding direction is reduced in Figure 2 as a result of the competing T_2 and T_2' effects. This is further illustrated in Figure 4, where the data acquired from the first echo train have darker regions between the regions of signal in column 90. When the frequency encoding direction is considered in the plot of row 96 in Figure 5, such a trend of higher contrast in the first echo acquisition is not apparent.

Discussion:

As the presented data suggest, the point spread function associated with intra-acquisition decay during EPI readouts is reduced on the ascending side of a spin echo due to the competing T_2 decay and T_2' rephasing. These effects yield a decay curve with a reduced slope during the readout, causing effective image-space convolution with a kernel that has a reduced point spread function. This phenomenon is primarily observed in the phase encoding direction because of the lower bandwidth during an EPI readout. The reduced point spread function in the phase encoding direction is apparent in column 90 of Figures 2 and 3, graphed in Figure 4, where the signal void is deeper when observed on the ascending side of the spin echo.

Interestingly, the same procedure performed on a human brain yields sharper images with later echoes. This is a result of the different T_2 decay times between the gray and white matter, leading to enhanced tissue contrast which overcomes the blurring associated with intra-acquisition decay, as seen in Figures 6 and 7 of the first and second echoes, respectively.

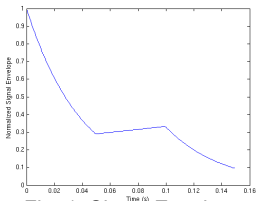

Fig. 1: Signal Envelope

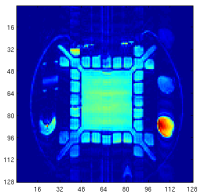
Fig. 2: Echo 1

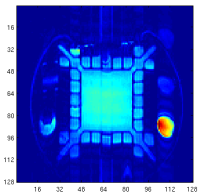
Fig. 3: Echo 2

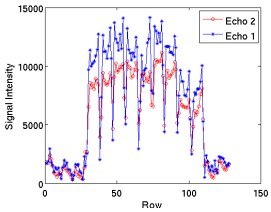

Fig. 4: Column 90

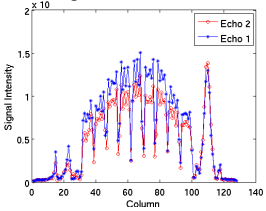

Fig. 5: Row 96

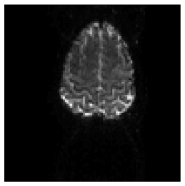
Fig. 6: Echo 1

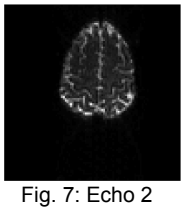
Fig. 7: Echo 2

References: [1] Farzaneh, et al. MRM 14: 123-139 (1990). [2] Jesmanowicz, et al. MRM 40:754-762 (1998). [3] Blaimer, et al. TMRI 15: 223-236 (2004). [4] Kim, et al. MRM 35: 895-902 (1996). [5] Kadah, et al. Proc. ISMRM 2004: 998.